CRDS line shape study of the (7 − 0) band of CO

Aleksandr A. Balashov,[1] Szymon Wójtewicz,[1] Jolanta Domysławska,[1] Roman Ciuryło,[1] Daniel Lisak,[1] and Katarzyna Bielska[1]

Institute of Physics, Faculty of Physics, Astronomy and Informatics, Nicolaus Copernicus University in Toruń, Grudziadzka 5, 87-100 Torun, Poland

(*Electronic mail: kbielska@umk.pl)

(Dated: 12 August 2024)

Abstract: We present the results of the spectral line shape study of the first measurement of the extremely weak $(7-0)$ band of the $^{12}C^{16}O$ molecule. Measurements were done with a highly sensitive cavity ring-down spectrometer. Collisional narrowing, analyzed in terms of speed-dependent effects, was observed for the first time for transitions with line intensities below $2 \cdot 10^{-29}$ cm/molecule at 296 K. We provide a full set of line-shape parameters of the speed-dependent and regular Voigt profile analysis for 14 transitions from P and R branches. Experimental verification of a strong vibrational dependence of the pressure shifting described by the Hartmann model [J.-M. Hartmann, JQSRT 110, 2019 (2009)] is extended up to the sixth overtone highly sensitive to the model parameter.

I. INTRODUCTION

Throughout the long history of molecular spectroscopy, carbon monoxide has emerged as a fundamental model system for investigating rotational and ro-vibrational transitions. Given its prevalence as the second-most abundant diatomic molecule following the molecular hydrogen in the interstellar medium, carbon monoxide holds substantial importance in the exploration of astrophysical environments. Carbon monoxide, in addition to satellite measurements, allows ground-based observations providing information about the molecular clouds[1,2] in which most stars are formed. CO is also present in the atmospheres of Venus[3,4], Mars[5,6] and exoplanets [7,8]. It is one of the gases used in human breath analysis for disease diagnostics[9].

Carbon monoxide is one of the major trace gases for biomass burning and fossil fuel combustion in the Earth's atmosphere[10,11]. With a lifetime of several weeks, it allows tracking of seasonal changes in air pollution[12,13]. It does not directly affect the global temperature[14] but plays an important role in atmospheric chemistry and controls the oxidative ability of the atmosphere[15,16]. The reaction of CO with the OH radical, which is the main sink of CO, affects the distribution and the amount of OH, which in turn significantly impacts the concentration of a variety of other trace gases (e.g. methane and other hydrocarbons as well as ozone)[17,18]. Many different satellite remote-sensing spectrometers such as MOPITT[19], ACE[20], and TROPOMI[21] and ground-based observatories like NDACC[22], TCOON[23] and COCCON[24] routinely monitor the concentration of CO in Earth's atmosphere.

Many experimental[25–44] and theoretical[45–49] works have been devoted to the spectroscopy of CO in the last decades. Significant progress in theoretical calculations of the line intensities has been shown on the example of the CO molecule[43]. However, purely quantum *ab initio* calculations are infeasible for systems larger than hydrogen, given current computational capabilities, despite their potential to accurately describe observed spectra.

Highly excited vibrational overtones of CO find applications in fundamental research as they are sensitive to the proton-to-electron mass ratio[50]. Hot bands of high vibronic states of CO were observed in stellar spectra [51–56], which helps to study the star formation processes. High-order overtones are challenging for laboratory studies due to the rapid decrease of their intensity with the increase of the vibrational quantum number of the upper level. It took more than four decades from the first measurements of CO emission hot bands up to $(6-4)$ and $(7-5)$ in an acetylene flame[57] in 1974 until the first measurement of the $(6-0)$ overtone band[38].

The calculated rotational distributions of intensities in the fundamental $(1-0)$ and low-overtone ($(2-0)$ and $(3-0)$) vibrational bands of carbon monoxide are nearly immune to the changes of the form of the potential-energy curves (PECs) and dipole-moment curves (DMCs). On the contrary, for high-$\Delta\nu$ overtones (where ν is a vibrational quantum number) Medvedev et al.[58] showed that line intensities are very sensitive to different approaches to calculating DMC. This situation indicated the need for experimental study of the sixth overtone unequivocally indicated by Meshkov et al.[48].

The sixth overtone of CO is located at the 690 nm wavelength region. Prior to this study, no measurements of $(7-0)$ band transitions were done. The line intensities measured in this work were reported in Ref.[49] together with the new *ab initio* calculations. The present paper reports all accompanying line-shape parameters: collisional broadening and shifting, and their speed-dependence parameters, which were out of the scope of the previous paper.

II. EXPERIMENTAL SETUP

Measurements are done with the optical frequency comb (OFC) assisted, Pound-Drever-Hall (PDH) locked, frequency-stabilized cavity ring-down spectrometer (FS-CRDS) in a similar configuration as the one used for the oxygen B-band study[59]. The principal scheme of our setup is shown in Fig. 1.

An external cavity diode laser (ECDL) from Toptica Pho-

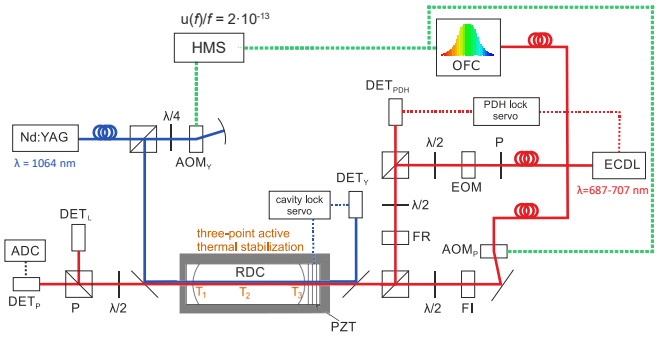

FIG. 1. Schematic diagram of the spectrometer. ECDL - probe laser, Nd:YAG - iodine stabilized reference Nd:YAG laser, OFC - optical frequency comb, HMS - hydrogen maser frequency standard, RDC - ring-down cavity, PZT - piezo transducer, AOM_Y, AOM_P - acousto-optic modulators, EOM - electro-optic modulator, DET_Y, DET_{PDH}, DET_L, DET_P - photodetectors, FI - Faraday isolator, FR - Faraday rotator, $\lambda/2$ and $\lambda/4$ - half- and quarter-wave plates respectively, P - linear polarizer, ADC - analog to digital converter. Solid lines indicate laser beams, whereas dotted lines mark servo loops and electrical signals.

tonics with the $687-707$ nm wavelength range is used as a radiation source for the measurement. The main laser beam is split into several beams. Two orthogonally polarised beams are coupled to the cavity. One of them is used for locking the laser frequency to the cavity mode, while the other serves as a probe beam. Locking the laser frequency to the cavity resonance with the PDH technique[60,61] not only increases frequency stability but also spectrally narrows the line width of the laser by more than two orders of magnitude below the cavity resonance width, allowing us to couple more light into the cavity.

The ring-down cavity is formed by double-wavelength-coated spherical mirrors in a non-confocal configuration. The cavity length is about 74 cm, and the corresponding free spectral range (FSR) is about 203 MHz. One of the mirrors is mounted on a piezo-transducer, which allows the stabilization of the cavity length by locking the comb of its eigenfrequencies to the frequency of a reference 1064 nm Nd:YAG laser. This laser provides long-term stability better than 5 kHz thanks to stabilization to the frequency of the I_2 hyperfine line. Moreover, such configuration allows controlled tuning of the cavity length to reduce the measurement frequency step below the FSR[62]. The intensity reflectivity of the mirrors is about $R = 0.96$ at 1064 nm corresponding to the Nd:YAG laser wavelength and $R = 0.999988$ for the probe beam. The latter was calculated from the measured ring-down time $\tau = 214$ μs for the empty cavity, at the 694 nm wavelength corresponding to the P8 line of $(7-0)$ band.

The temperature of the cell was actively stabilized at 296.000(35) K with three-point gradient equalization with a measured gradient at the level of 18 mK[59]. The temperature was measured with three Pt100 resistance temperature detectors (RTD), placed at both ends and in the center of the cavity, while two additional RTDs, placed between them, were used to monitor the residual temperature gradient. The standard uncertainty of the temperature measurement of 30 mK resulted from calibration against two reference Fluke type 5641 thermistors with 1 mK manufacturer-stated calibration uncertainty and less than 7 mK long-term drift in 4 years.

For pressure measurement a Wika CPG2500 pressure sensor from Mensor, with the manufacturer's full range (900 Torr) stated accuracy of 0.08‰ was used. An additional comparison with another sensor of the same model revealed that the overall pressure measurement uncertainty amounts to 0.13‰, including laboratory temperature fluctuations.

The optical frequency was measured with the OFC referenced to the 10 MHz radio frequency (RF) signal[63,64] (relative stability[65] of $2 \cdot 10^{-13}$ at 1 s) from hydrogen maser[66] located at the Astro-Geodynamic Observatory (AOS) in Borowiec, Poland and transferred to our laboratory by a fiber link.

III. MEASUREMENTS AND DATA ANALYSIS

In total 14 distinct lines originating from the P and R branches within the CO $(7-0)$ band were chosen for the study using a carbon monoxide sample at natural isotopic abundance with stated purity of 99.997%. Each line was measured at five pressures from 50 Torr (6.7 kPa) to 750 Torr (100 kPa) for ten stronger (P13, P12, P11, P10, P9, P8, P7, P4, R4 and R6) lines, and from 100 Torr (13.3 kPa) to 800 Torr (106.7 kPa) for four weaker (P19, P16, P1, and R0) lines. These specific lines were chosen with a deliberate emphasis on isolation, ensuring minimal overlap with residual H_2O and O_2 spectra. Our selection process aimed to encompass a wide range of rotational quantum numbers, J, to determine J-dependencies of line-shape parameters. Spectral regions close to the line center were measured with four points per FSR, making the frequency step nominally about 50 MHz, and line wings were measured with a frequency step equal to one FSR. The total scan width was about 30 GHz, which was necessary to properly record and analyze the spectra baseline at various pressures, see Section III B for more details. For each pressure, typically 20 scans (from 14 to 88, depending on the absorption) were averaged.

A. Line profile

For the analysis of the experimental spectra we used the Voigt profile (VP), the speed-dependent Voigt profile[67] with quadratic approximation[68] for the speed dependence (qSDVP), and the quadratic speed-dependent Nelkin-Ghatak profile (qSDNGP)[69–71]. These profiles are well-known limits of the Hartmann-Tran profile (HTP)[71] recommended by IUPAC[72] and implemented in HITRAN[73]. The speed dependence of collisional width Γ and shift Δ in qSDVP and qSDNGP is accounted for within the quadratic approxima-

tion:

$$\Gamma(x) = \Gamma_0\left(1 + a_W\left(x^2 - \frac{3}{2}\right)\right),$$
$$\Delta(x) = \Delta_0\left(1 + a_S\left(x^2 - \frac{3}{2}\right)\right), \quad (1)$$

where x is reduced absorber velocity $x = \upsilon/\upsilon_0$, υ_0 is the most probable absorber velocity, $a_W = \Gamma_2/\Gamma_0$ and $a_S = \Delta_2/\Delta_0$ are dimensionless parameters describing the speed dependence of Γ and Δ, respectively. Other line-shape parameters use the same notation as in Ref.[71].

To minimize the cross-correlation between the fitted line-shape parameters, the multispectrum fitting procedure[74,75] was used. All baseline parameters were fitted as individual parameters for different pressures, while unperturbed line position, ν_0, the speed dependence of pressure broadening, a_W, and shifting, a_S, were common. Pressure-independent Doppler width was fixed at the value calculated from the temperature measurement. Γ_0 and Δ_0 were assumed to linearly depend on pressure for the given temperature, thus pressure independent coefficients, Γ_0/p and Δ_0/p, were fitted. Two approaches were used with respect to the line intensity S. First, which in this paper we will refer to as the individual line area (ILA) approach, where the line area, A, was fitted in the multifit procedure as an individual parameter for each pressure. The dependence of the line area on concentration was later fitted with a linear function, i.e. $S \propto A/p$, to determine the line intensity. In the second approach, referred to as the linear line area (LLA) approach, the line area was fitted as a coefficient proportional to the concentration, common for all pressures instead. The ideal gas approximation was adopted both in the ILA and LLA approaches, and the line intensity was calculated from the fitted A/p coefficient. The latter approach is considered to be more robust as it reduces the number of fitted parameters in the model, thus the correlation between parameters, while the ILA approach provides a sensitive test to the possible non-linearity of the determined line area on the pressure.

Fig. 2 shows averaged spectra of one of the strongest lines − P8, measured at the pressure of 225 Torr together with fit residuals from the VP (red line) and qSDVP (black line) fits shown on bottom panel. The analysis of the spectra with a simple Voigt profile (neglecting speed-dependent effects: a_W and $a_S = 0$) resulted in a characteristic W-shape of the fit residuals indicating that VP cannot accurately model the spectrum. The insufficiency of VP was not so pronounced for all the lines and pressures as it gets masked by the experimental noise. However, we noticed the nonlinear dependence of the area on the pressure for the VP fits with the ILA approach, which is not expected at this level in this pressure range. It was observed for some of the lines, presented in Fig. 3. Other transitions for which this effect was not observed have relatively low intensity with one exception − the R6 transition. Similar nonlinear behavior of line intensities determined with VP was previously observed for H_2O lines[76]. Simulating the spectra for the conditions of the experiment with qSDV and qSDNG profiles, accounting for the speed dependence of collisional

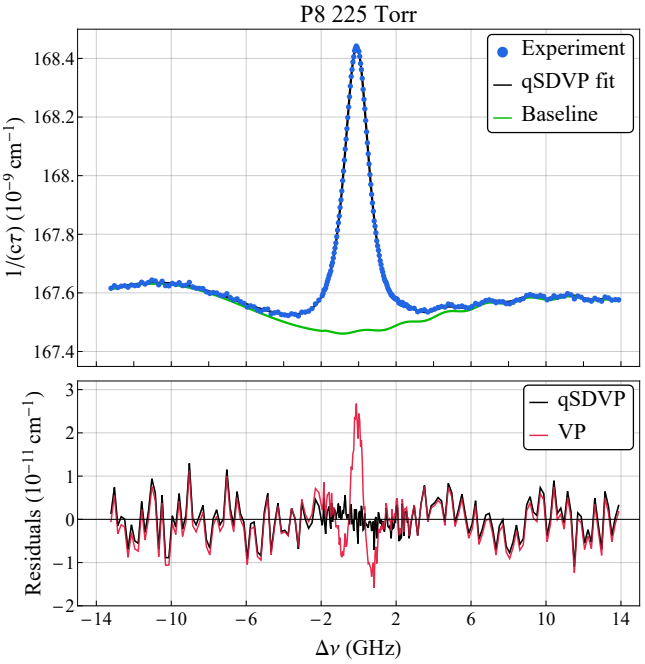

FIG. 2. Top panel: averaged spectra of the P8 line at 225 Torr shown with blue dots (●), black line - fitted qSDV profile, green line - fitted baseline. Bottom panel: fit residuals for the VP (red line) and qSDVP (black line) analysis.

width and shift, and comparing the results of analysis of simulated data with different profiles with and without the speed dependence in the ILA approach confirmed that such nonlinear behavior of the line area on the pressure is the artifact of an incorrectly chosen line profile. Such behavior means that the determined line intensity would depend on the pressure range of the measurements if VP with LLA had been used and, for the case of experimental data, leads to the underestimation of the line intensities by 1.2% on average compared to the qSDVP LLA results. Systematic nonlinear behavior of the line area over pressure for VP fits suggested that the use of a more advanced line profile is necessary for this data, regardless of the relatively low signal-to-noise (SNR) ratio for the single pressure spectra, which was only up to about 300 for the strongest transitions at the highest pressures.

Comparison of fit results of qSDNGP and qSDVP analysis showed that qSDVP sufficiently well models experimental data. The use of a more advanced qSDNG profile, that takes into account the frequency of the velocity-changing collisions described by the hard collisions model[77] and resulting Dicke narrowing effect[?], led to larger uncertainties of line parameters. This was caused by the increased number of fitted parameters and higher cross-correlation between them, especially between a_W, responsible for the line narrowing due to the speed dependence, and ν_{VC}/p, responsible for the line narrowing due to the velocity-changing collisions[78,79]. The effect of the correlation is visually demonstrated in Fig. 4, where there are shown values of ν_{VC}/p coefficient from the results of qSDNGP LLA fits of the P8 line with the a_W pa-

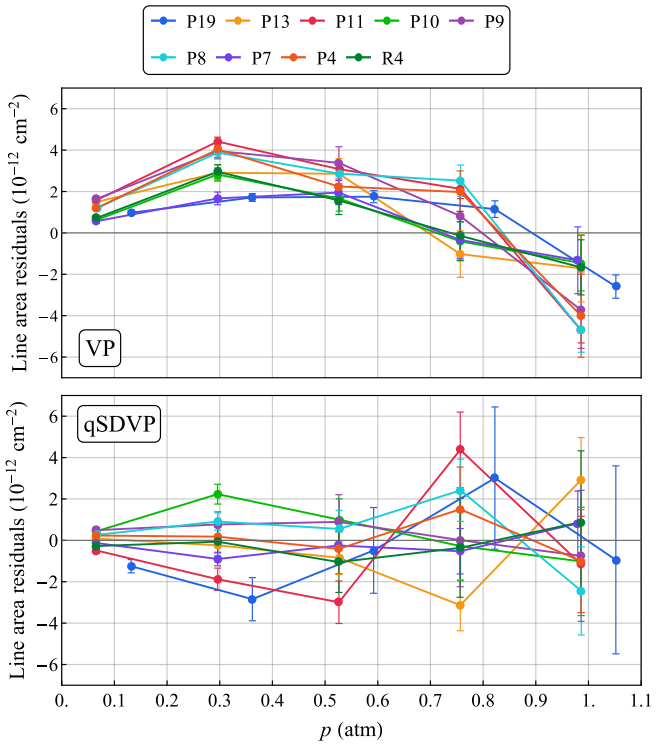

FIG. 3. Residuals of the linear fit of the dependence of area on the pressure for VP ILA (top panel) and qSDVP ILA (bottom panel), for lines indicated with different colors as in the legend. Uncertainty intervals show only type A standard uncertainty. Details in Section III A.

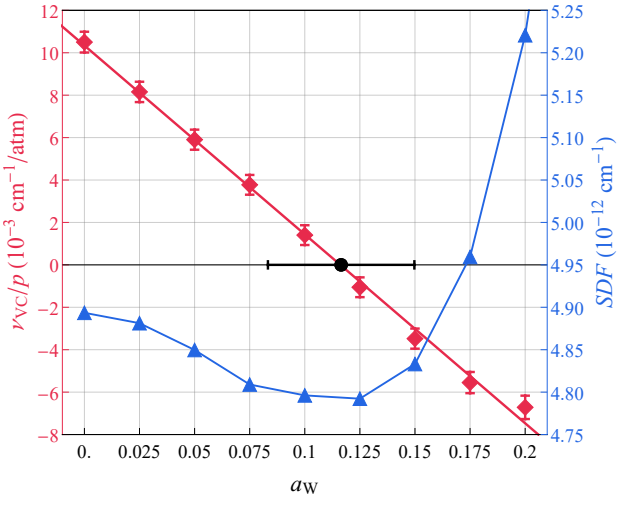

FIG. 4. Overlaid plots of ν_{VC}/p (◆) and SDF (▲) (Eq. (2)) against a_W illustrate the correlation between a_W and ν_{VC}/p. The results obtained from qSDNGP LLA fit of the P8 line with fixed values of a_W, plotted along the horizontal axis. The red line is a linear fit of the ν_{VC}/p data. Uncertainty bars for qSDNGP results show only type A standard uncertainty. The fitted value of a_W from qSDVP LLA fit is shown with a black dot (●) with an uncertainty bar representing total experimental standard uncertainty. Details in Section III A.

rameter being fixed to different values together with a corresponding standard deviation of the fit residuals (SDF):

$$SDF = \sqrt{\frac{\sum_i^W \left(\alpha_{exp}(\nu_i) - \alpha_{fit}(\nu_i)\right)^2}{W - r}}, \tag{2}$$

where α_{exp} and α_{fit} are values of the absorption coefficients measured in the experiment and calculated with the fitted profile, respectively, W is the total number of experimental points, and r is the number of fitted parameters in the model. Fig. 4 shows a strong correlation between ν_{VC}/p and a_W. It also shows that the best fit (corresponding to the minimal SDF value) is obtained for the values of ν_{VC}/p close to zero. Fitting qSDNGP, with both ν_{VC}/p and a_W as floating parameters for most of the lines, resulted in ν_{VC}/p values equal to zero within their standard deviations. Nonetheless, taking into account a very strong correlation between parameters characterizing the speed dependence of collisional broadening and Dicke narrowing, as well as a relatively low signal-to-noise ratio, we opted not to ascertain the relative importance of both effects. Consequently, for the conclusive analysis, we selected the qSDVP model, employing the LLA approach for multispectrum fitting. This model describes all narrowing using solely the a_W parameter, even if its origin in part can be due to the Dicke narrowing effect.

Derived qSDVP LLA line-shape parameters are listed in Table I. Because the Voigt profile is used in many applications, we provide an additional set of parameters (see Table II) arising from the VP LLA fits, for which etalon parameters (See section III B for the details) were fixed to the values from qSDVP fits to minimize the effect of the baseline on the line shape. The VP has fewer floating parameters, and only line-shape parameters together with constant offset and linear slope of the baseline were optimized for VP analysis. This makes a significant difference in the total number of floating parameters in the case of the multispectrum fit compared to the qSDVP case, which explains the fact that for some of the weaker lines, their quality-of-the-fit factors (QFs)[80,81] are higher for VP than for qSDVP.

In addition to the 14 explicitly stated transitions, we identified the R22 line, which was only partially recorded because it was situated on the edge of the spectra of the R6 line. Attempting to derive meaningful values for a_W and a_S under these circumstances proved unfeasible, resulting in excessively large uncertainties. To address this, we constrained their values to the corresponding averages derived from other recorded lines (from P19 to R4). Line parameters for R22 are provided in Tables I and II but are excluded from all figures for visual clarity as well as from the discussion and conclusions. The positive pressure shifting observed in the R22 line is likely an artifact arising from its incomplete recording. It is highly improbable that the actual value of pressure shifting coefficient is inherently positive.

TABLE I. Line-shape parameters from qSDVP LLA fit. Unperturbed line position, ν_0, is given in cm^{-1}, line intensity, S, is in units 10^{-30} cm/molecule, collisional broadening, Γ_0/p, half width at half-maximum (HWHM), and shifting, Δ_0/p, coefficients are in cm^{-1}/atm at reference temperature T_{ref} = 296 K. Speed-dependence parameters a_W and a_S are dimensionless. Uncertainties given in parentheses are total experimental standard uncertainties (1σ) in units of the last digit quoted. QF is the quality-of-the-fit factor.

Line	ν_0	S	Γ_0/p	Δ_0/p	a_W	a_S	QF
P19	14334.40122(84)	1.81(38)	0.0616(107)	-0.0193(28)	0.065(44)	0.08(15)	36
P16	14358.36237(42)	3.65(27)	0.0624(26)	-0.0168(14)	0.124(36)	0.17(12)	76
P13	14380.14082(29)	6.70(27)	0.0653(19)	-0.0173(10)	0.087(35)	0.33(12)	124
P12	14386.91468(23)	7.53(31)	0.0656(19)	-0.0164(9)	0.080(35)	0.08(12)	136
P11	14393.44482(35)	9.07(37)	0.0683(22)	-0.0190(9)	0.103(35)	0.34(12)	138
P10	14399.73166(19)	9.59(35)	0.0677(18)	-0.0165(8)	0.102(34)	0.12(12)	190
P9	14405.77460(18)	10.65(36)	0.0698(17)	-0.0163(8)	0.098(34)	0.13(12)	184
P8	14411.57391(15)	10.99(37)	0.0714(17)	-0.0151(7)	0.117(34)	0.10(12)	249
P7	14417.12981(16)	11.03(37)	0.0728(17)	-0.0152(7)	0.131(34)	0.12(12)	248
P4	14432.33271(22)	8.45(32)	0.0778(20)	-0.0132(9)	0.086(34)	0.14(12)	157
P1	14445.33617(63)	2.54(27)	0.0939(57)	-0.0128(18)	0.092(46)	0.31(23)	37
R0	14452.78145(69)	2.46(28)	0.0899(65)	-0.0110(19)	0.064(44)	0.50(24)	42
R4	14464.72911(21)	9.12(32)	0.0746(17)	-0.0144(7)	0.115(34)	0.23(12)	183
R6	14469.22876(18)	9.99(34)	0.0689(16)	-0.0144(7)	0.078(34)	0.14(12)	168
R22	14469.70244(423)	0.89(32)	0.0876(131)	0.0119(97)	0.100[a]	0.18[a]	12

[a] a_W and a_S for the R22 line fitting were fixed to the weighted average values, with the weights inversely proportional to the variance of the value, from the results of the other lines (from P19 to R4). Details in the Section III A.

TABLE II. Line-shape parameters from the VP LLA fit. Unperturbed line position, ν_0, is given in cm^{-1}, line intensity, S, is in units 10^{-30} cm/molecule, collisional broadening, Γ_0/p (HWHM), and shifting, Δ_0/p, coefficients are in cm^{-1}/atm at reference temperature T_{ref} = 296 K. Uncertainties given in parentheses are total experimental standard uncertainties (1σ) in units of the last digit quoted. QF is the quality-of-the-fit factor.

Line	ν_0	S	Γ_0/p	Δ_0/p	QF
P19	14334.40136(84)	1.78(38)	0.0597(107)	-0.0191(28)	41
P16	14358.36250(42)	3.59(27)	0.0599(26)	-0.0161(14)	77
P13	14380.14098(29)	6.64(27)	0.0639(19)	-0.0161(10)	124
P12	14386.91475(23)	7.45(31)	0.0640(19)	-0.0162(9)	144
P11	14393.44512(35)	8.97(37)	0.0666(22)	-0.0177(9)	130
P10	14399.73176(19)	9.47(35)	0.0656(18)	-0.0162(8)	178
P9	14405.77470(18)	10.52(36)	0.0678(17)	-0.0159(8)	178
P8	14411.57398(15)	10.82(37)	0.0688(17)	-0.0148(7)	204
P7	14417.12989(16)	10.83(37)	0.0696(17)	-0.0147(7)	194
P4	14432.33278(22)	8.36(32)	0.0760(20)	-0.0128(9)	160
P1	14445.33632(63)	2.51(27)	0.0916(57)	-0.0119(18)	43
R0	14452.78171(69)	2.45(28)	0.0889(65)	-0.0103(19)	48
R4	14464.72924(21)	8.99(32)	0.0721(17)	-0.0137(7)	164
R6	14469.22885(18)	9.88(35)	0.0672(17)	-0.0140(7)	173
R22	14469.70255(415)	0.85(37)	0.0833(131)	0.011(10)	12

B. Spectra baseline

Raw spectra consist of CO absorption lines (whose absorption in the line center was $0.07\% - 0.6\%$ of the total losses) and the baseline that represents losses not related to absorption in the gas. The baseline was modeled with a linear function comprising two parameters: a constant offset and a slope, accounting for possible changes in mirrors reflectivity and sine functions, accounting for the etalons (See next paragraph). The amplitude of the baseline function observed on the spectra was comparable to the amplitude of the line. This required a detailed investigation of the influence of the baseline model on determined line parameters. Averaged spectra at different pressures with corresponding etalons in the baseline and fit residuals on the example of the P10 line are shown in Fig. 5.

Interference between light oscillating inside the ring-down cavity (formed by the internal reflective surfaces of cavity mirrors) and the light reflected back from weakly reflective surfaces outside the main cavity caused sinusoidal modulation of the spectra baseline. This effect is known as an etaloning effect[82,83]. We observed at least two etalons in our spectra with periods of about 26 GHz and 17 GHz corresponding to the reflection from the external surfaces of cavity mirrors and from the cell windows, respectively. Those etalons were modeled with a simple sine function with parameters fitted individually for each pressure. Additionally, we noticed a quasi-

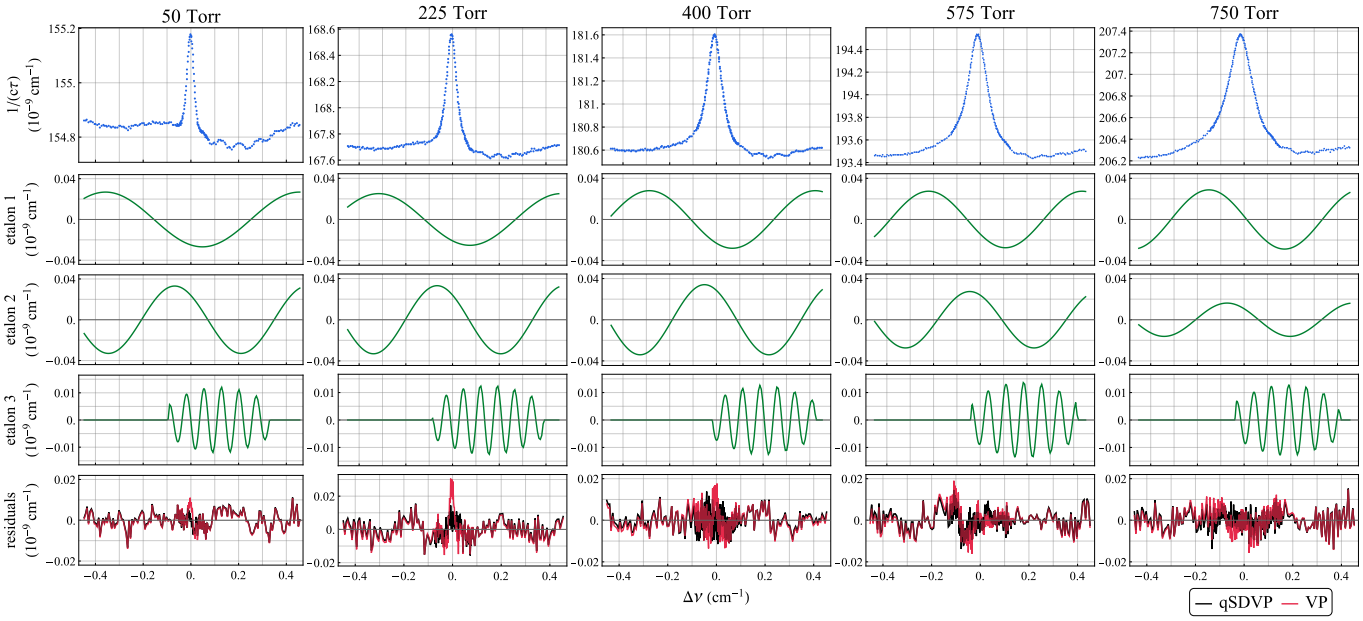

FIG. 5. P10 line of $(7-0)$ band of CO measured at five different pressures at temperature of 296 K. Top row shows raw averaged spectra with nominal pressures indicated above. Fitted etalons are shown in rows No 2, 3, and 4. The bottom row shows fit residuals from LLA fit for qSDVP in black and for VP in red. The horizontal axis shows the frequency detuning $\Delta\nu$ from the unperturbed line position. Details in Section III B.

periodical signal, which will be referred to in this paper as the third etalon, with a period of 2.5 GHz covering only part of a spectrum (see Fig. 5). Half-period of 1.3 GHz is close to the line width at low pressures as the Doppler width is about 1 GHz, and the collisional width for the experimental conditions varied between 0.25 GHz and 6 GHz. This made the third etalon a potential source of significant systematic uncertainty. Such quasi-etalon spectrum may be a consequence of several interfering etalons with different periods. Contrary to the first two etalons, formed by parasitic reflections from surfaces located inside the temperature-stabilized enclosure, the third etalon is partially formed by elements outside of the thermal enclosure, which leads to changes in its parameters (mainly the phase) during measurements. To model the third etalon, its approximating function was modified by a smooth envelope made from a half-period-part of cosine function between zeros and equal to zero elsewhere and characterized by its effective width and position. This form was chosen from considerations of possible beat note of two etalons with equal amplitudes and the difference between periods of about 2.5 GHz. While regular cosine envelope function could potentially account for the observed 2.5 GHz etalon's amplitude modulation, it would create similar increasing and decreasing oscillations after the envelope crossed the zero level. However, this was not in accordance with the patterns observed in the spectra. To address this inconsistency, we made the decision to utilize only one half-period segment of the envelope function and set it to zero elsewhere. It is important to note that this peculiar behavior may be attributed to an artifact of temporal variations of the frequency and the phase of the third etalon and the consequent averaging of numerous scans conducted over an extended time span for a single pressure measurement (lasted on average nine hours) rather than being intrinsic characteristics of the etalon itself.

C. Uncertainties estimation

Parameters uncertainties presented in Tables I and II are the total experimental standard uncertainty (1σ) determined by accounting for all considered contributions according to Table III where a detailed breakdown of the corresponding contributions to the uncertainty budget for LLA qSDVP parameters is shown on the example of the P10 line.

For the estimation of systematic uncertainties due to the fitting procedure, the maximal difference of parameters from ILA and LLA multispectrum fit approaches of qSDVP was divided by $\sqrt{3}$ as it is advised[84] to consider a rectangular distribution as an alternative assumption, given that systematic deviations are unlikely to follow a normal distribution. The resulting relative systematic uncertainty contributed from 0.11% to 16% to the total relative standard uncertainty of line intensity, depending on the transition, and up to $1.7 \cdot 10^{-4}$ cm^{-1} (5.2 MHz) to the uncertainty of the unperturbed line position.

To determine the impact of the baseline on the uncertainty of the fitted line parameters, a set of simulations was made with over one hundred configurations of observed etalons and line profiles. We estimated how using different line profiles together with different phases of etalons relative to the line center would affect retrieved parameters values for the conditions of the experiment. All simulations were done for two levels of SNR corresponding to the strongest and the weakest measured

TABLE III. Detailed uncertainty budget of the qSDVP parameters for the P10 line. Contributions to the standard uncertainty of the unperturbed line position, ν_0, are given in 10^{-3} cm^{-1}, contributions to the standard uncertainties of all other parameters are given as relative values except for the a_W and a_S, for which it is absolute and dimensionless.

Parameter	ν_0	S	Γ_0/p	Δ_0/p	a_W	a_S
Type A uncertainty	0.067	0.003	0.0038	0.0095	0.0062	0.022
Contribution to B type uncertainty:						
frequency reference accuracy	0.000015	0.00008	0.00015	0.00071	—	—
temperature measurement accuracy	—	0.00012	0.00012	0.00012	—	—
temperature dependence	—	0.00032	0.00006	0.00006	—	—
pressure measurement accuracy	—	0.00013	0.00013	0.00013	—	—
approach to multispetrum fitting (ILA or LLA)	0.033	0.016	0.016	0.012	0.021	0.0003
repeatability	0.029	0.018	0.019	0.037	0.0075	0.075
baseline model	0.14	0.025	0.012	0.025	0.025	0.082
Total uncertainty	0.17	0.034	0.027	0.05	0.034	0.12

transitions, giving us the ability to linearly scale corresponding uncertainties for all measured spectra. Baseline-related uncertainty contributed from 2.2% up to 13% to the total relative standard uncertainty of the line intensity. It contributed from $1.3 \cdot 10^{-4}$ cm^{-1} to $8 \cdot 10^{-4}$ cm^{-1} (3.7 to 23 MHz) of line position, depending on the transition. Uncertainty related to the baseline model was the main uncertainty component for the line intensity, the unperturbed line position, and the speed dependence of the pressure broadening coefficient.

Additionally, in order to not underestimate the total uncertainty, we include the contribution from the comparison of repeated measurements for the P8 line as an example. Subsequent measurement was done in the same way for all pressures more than one month after the first one.

The line mixing effect should not affect the line intensity of CO on a level higher than 0.26%. This was calculated by fitting qSDVP to the spectra simulated with qSDVP with line mixing. Spectra were simulated using the maximal absolute value of the first order[85] line mixing coefficient Y = 0.02 atm^{-1} from the HITRAN2020 database[86] for the CO $(7-0)$ band, and maximal values of pressure broadening and shifting coefficients observed in the experiment with the noise level typical for the experiment. This error is safely below the stated total standard uncertainty.

For pressure shifting and its speed-dependence parameter most of the uncertainty came from the measurement repeatability and the influence of the baseline. Pressure-broadening uncertainty originated evenly from the systematic uncertainty, repeatability, and the impact of the baseline.

For the VP LLA results presented in Table II the total experimental uncertainty (in parentheses) for unperturbed line position and line intensity, include also uncertainty associated with the choice of the line profile. It was estimated by comparing the results of the qSDVP LLA fit and the VP LLA, for which the etalons parameters were fixed to the values from qSDVP spectra analysis. The choice of the line profile contributed from 0.6% up to 1.8% to the total relative standard uncertainty of the line intensity and from $0.7 \cdot 10^{-4}$ cm^{-1} to $3 \cdot 10^{-4}$ cm^{-1} (2 to 9 MHz) of the line position, depending on the transition. Other parameters are not directly comparable for considered profiles.

Type A uncertainty was always smaller than type B for all transitions and parameters. We acknowledge that some components of the uncertainty are not completely independent and thus partially account for the same source of uncertainty. Nonetheless, we prefer to overestimate the uncertainty rather than underestimate it by neglecting any of the components.

IV. RESULTS AND DISCUSSION

A. Comparison with available theoretical data

All determined line-shape parameters are presented in Tables I and II, resulting from the qSDVP fits with the LLA approach and from the VP LLA fits, respectively. Fig. 6 displays all the results, where values determined with the qSDVP LLA approach, indicated with black dots (●), and VP LLA, indicated with red triangles (▲), are compared with data from the HITRAN2020 database[86,87] for qSDVP, marked with empty rectangles (□), and for VP, marked with green rectangles (■), plotted against the line index m. Line index m is defined as follows: $m = -J''$ for the P branch and $J''+1$ for the R branch, where J'' is the rotational quantum number of the lower state of the CO molecule. Note that the line intensities and unperturbed line positions for VP and qSDVP in HITRAN2020 are exactly the same data. The experimental results for the qSDVP and VP analysis agree with each other within their total standard uncertainty.

Line positions and intensities given in HITRAN2020 are taken from the semi-empirical calculation of Li et al.[47]. This calculation is based on the PEC of Coxon and Hajigeorgiou[45] and the DMC combined from a fit of the best available at that time, experimental data of transitions from $(0-0)$ up to $(6-0)$ bands and spline-interpolation of their *ab initio* DMC.

Panel a) of Fig. 6 shows absolute values of the line intensities of measured transitions. Comparison with HITRAN2020 data shows that calculations significantly underestimate intensities, and the experimental values are approximately two times higher.

The difference between measured values of unperturbed line positions and values from HITRAN2020 is shown in

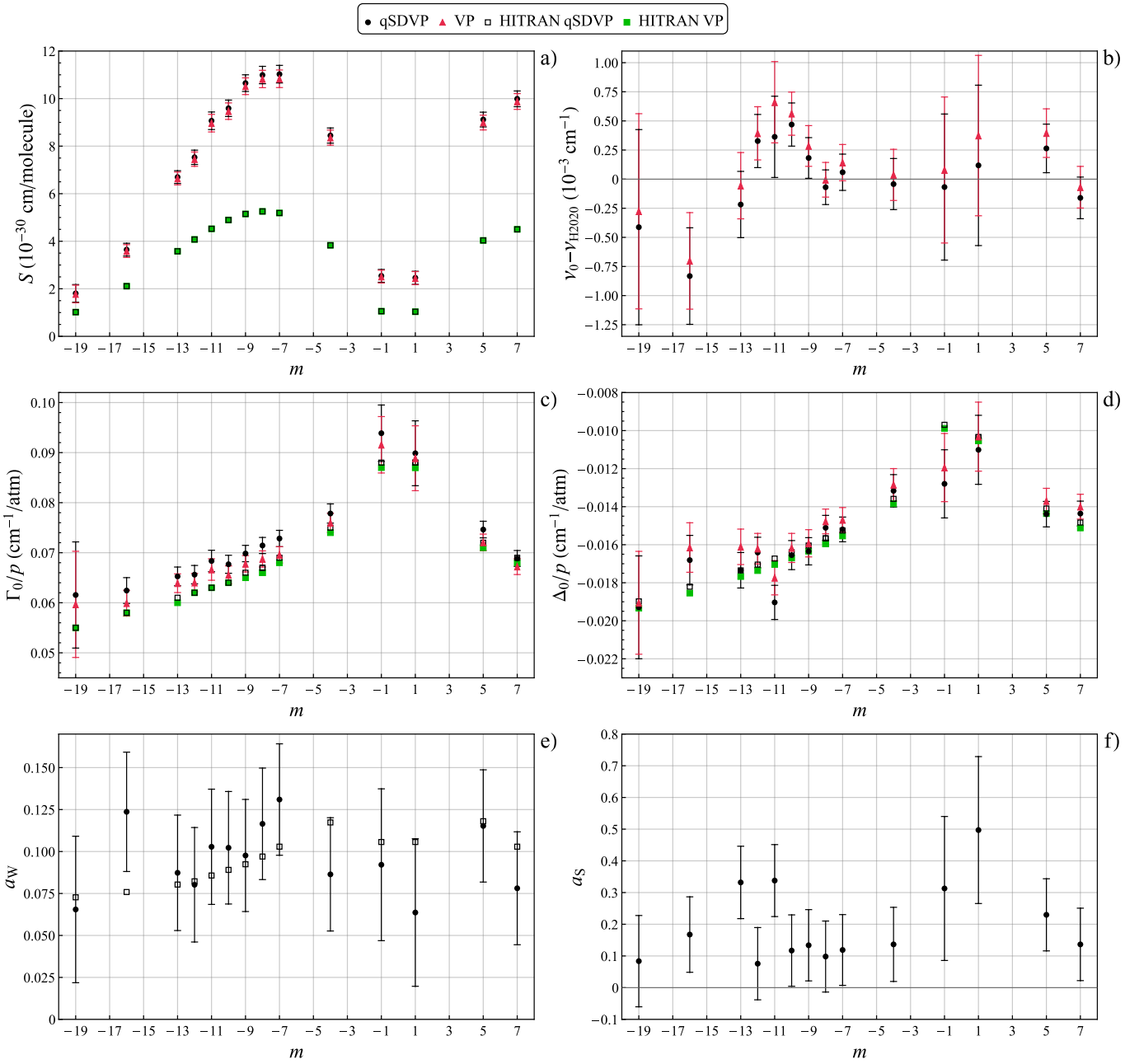

FIG. 6. Comparison of experimental values from the qSDVP LLA (●) and VP LLA (▲) analysis of all determined line parameters with data from HITRAN2020 database[86,87] for qSDVP (□) and VP (■) against line index m. Panel a) shows absolute values of line intensities, and panel b) shows the difference between determined line positions and corresponding values ν_{H2020} from the HITRAN2020 database. Comparisons of absolute values of pressure broadening (HWHM) and shifting are shown in panels c) and d), respectively. Panel e) shows a comparison of the speed dependence of pressure broadening parameter, a_W, for qSDVP fit and data available in the HITRAN2020 database. For the speed dependence of pressure shifting, a_S, only qSDVP data from this work is available and shown in panel f). Uncertainty bars on the experimental data points correspond to the total standard uncertainty. Details in Section IV A.

panel b) of Fig. 6. Experimental values agree with the calculation within one standard uncertainty for most of the lines and within two standard uncertainties for all of the measured lines.

We should mention that no direct calculations for the line-shape parameters (other than line position and intensity) nor measurements are available for considered transitions of $(7-0)$ band. The comparison of pressure broadening with HITRAN2020 would show only consistency across different bands. This is because the HITRAN2020 VP data is a Padé approximation of the best available at that moment measurements of the lower bands[87] (only up to the $(4-0)$), while qSDVP data is an approximation of measurement of $(2-0)$

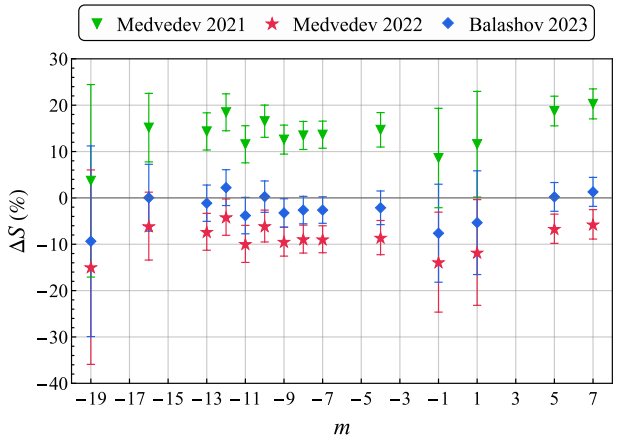

FIG. 7. The relative differences of the theoretical line intensities from the experimental data, determined with Eq. (3). The calculations of Medvedev and Ushakov from 2021[58] and 2022[88] are indicated with green (▼), and red (★)[88]symbols, respectively. The calculations of the UCL group[49] are shown in blue (◆).

band by Devi et al.[34]. Although it has been observed that pressure broadening for those transitions remains relatively independent of the branch and the band[87], it should not be automatically assumed that the same holds true for higher overtone transitions. The self-induced pressure shifting coefficients in HITRAN2020 are based on measurements of the fundamental band and the first two overtones[87] for the VP case and on the measurement of $(2-0)$ band by Devi et al.[34] for the qSDVP case, see details in Section IV B.

Our measured values of the collisional self-induced pressure broadening coefficient, Γ_0/p, show good repeatability of the shape of its dependence on the line index m in comparison with HITRAN data, but calculations seem to underestimate the absolute values by about 5% on average, see panel c) of Fig. 6. Also, Γ_0/p values of the R branch seem to agree better with predicted values than for the P branch. Panel d) of Fig. 6 shows the pressure shifting coefficient, Δ_0/p. Its values are in agreement with HITRAN2020 data within total standard uncertainty for most of the transitions. The results for a_W (panel e) of Fig. 6) are in agreement within the total standard uncertainty with calculations and are able to reflect the general shape of its m dependence. This fact additionally supports the use of the qSDVP for the final analysis. The qSDVP implementation in HITRAN2020 assumes only speed dependence of pressure broadening and no speed dependence of pressure shifting. Therefore, in the panel f) of Fig. 6 only results of this work are shown.

In Fig. 7 we compare our measured line intensities with more recent calculations. The relative differences of line intensities of different theoretical calculations from the experimental values are calculated according to the formula:

$$\Delta S = \frac{S_{\text{Theoretical}} - S_{\text{Experimental}}}{S_{\text{Experimental}}} \cdot 100\%. \qquad (3)$$

Calculations of Medvedev and Ushakov using DMF constructed with irregular functions and 16 adjustable parameters[58], shown with green triangles (▼), predicted roughly two times higher values of line intensities of $(7-0)$ band transitions than the HITRAN2020. They are higher by 14% on average from the experimental ones. Refined calculations of the same authors with irregular DMF and 13 adjustable parameters[88], shown with red star symbols (★), predicted line intensities even closer to the experimental values, only 9% on average smaller than the measured ones. However, the new calculations from the theoretical group in University College London[49], shown with blue diamond symbols (◆), yield the best agreement with the experiment. It matched experimental values of almost all line intensities within one standard experimental uncertainty. Calculated intensities are smaller than the experimental ones by 2.4% on average. The calculations are based on a similar approach that gave sub-promille accuracy in determining line intensities of $(3-0)$ band[43]. For a detailed discussion of the results on line intensities and issues that accompanied the new theoretical calculations, we send the reader to our recent paper[49].

B. Comparison of (7 − 0) broadening and shifting coefficients with other CO bands

Fig. 8 shows a comparison of our values of self-induced pressure broadening coefficients from the VP LLA fit (top panel) and the qSDVP LLA fit (bottom panel) with available experimental data for the pure rotational band $(0-0)$, fundamental ro-vibrational band $(1-0)$ and overtones of CO up to $(6-0)$. The results of measurements of the $(2-0)$ band by Predoi-Cross et al.[89] and Devi et al.[34] are not shown on the top panel of Fig. 8, as they are in perfect agreement with more recent measurement by Esteki et al.[39](△). The results of the $(3-0)$ band by Swann et al.[30], not shown on the top panel of Fig.8, agree within the margin of uncertainty with the results of Predoi-Cross et al.[32] (×). Our values (●) of pressure broadening coefficients obtained with the VP fit are within the scatter of experimental values for fundamental and lower overtone bands. However, our qSDVP results (bottom panel of Fig. 8) are slightly higher on average than the results for other bands. For certain values of m, they diverge by more than one experimental uncertainty from other measurements. However, it is worth noting that, for the results of Tretyakov et al.[44] (⋆), Wójtewicz et al.[35] (×), $(4-0)$ band results of Borkov et al.[40] (○) and for this work (●), uncertainty bars on the bottom panel of Fig. 8 show total standard experimental uncertainties (1σ) while for all the others only statistical (1σ) uncertainty from the fit, as the rest of the authors did not provide estimation of their type B uncertainties.

Fig. 9 shows our qSDVP LLA values (●) of self-induced pressure shifting coefficients, Δ_0/p, together with measurements for lower overtones, fundamental and pure rotational bands from the literature in comparison with theoretical values of Δ_0/p for qSDVP and VP, shown with solid lines and dashed lines respectively. Experimental data from Tretyakov

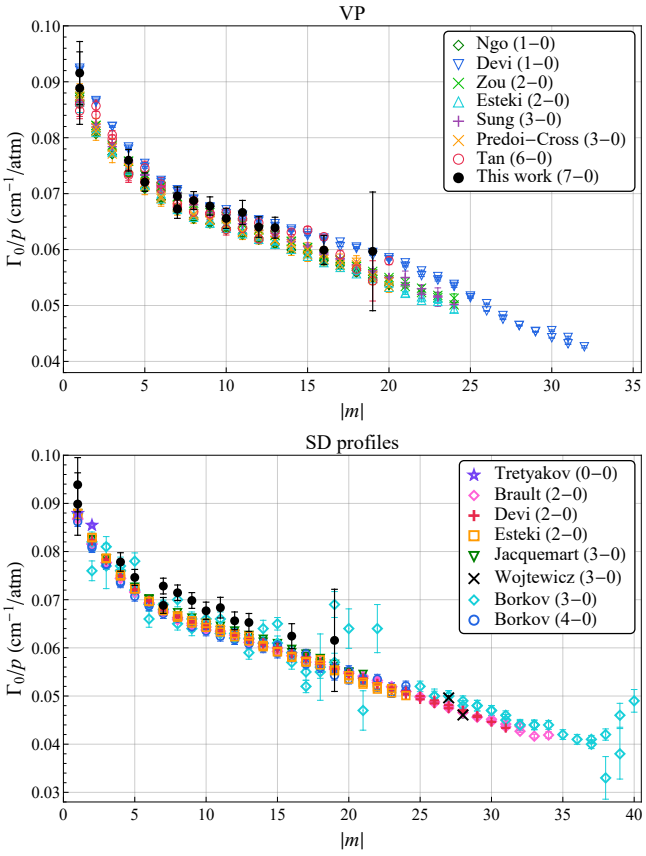

FIG. 8. Top panel: The measured self-induced pressure broadening coefficients versus absolute values of the line index m from the VP analysis. The values from this work for the $(7-0)$ band (●) are compared to the values for $(1-0)$ band by Ngo et al.[36] (◇) and Devi et al.[26] (▽), $(2-0)$ band by Zou and Varanasi[29] (×) and Esteki et al.[39] (△), $(3-0)$ band by Sung and Varanasi[31] (+) and Predoi-Cross et al.[32] (×), and $(6-0)$ band by Tan et al.[38] (○). Bottom panel: The measured self-induced pressure broadening coefficients versus absolute values of the line index m from the analysis with profiles accounting for the speed dependence of pressure broadening. The values from this work for the $(7-0)$ band (●) are compared to the values for pure rotational $(0-0)$ band by Tretyakov et al.[44] (☆), $(2-0)$ band by Devi et al.[34] (+) and Esteki et al.[39] (□), $(3-0)$ band by Jacquemart et al.[28] (▽) , Wójtewicz et al.[35] (×) and Borkov et al.[41] (◇), and $(4-0)$ band by Borkov et al.[40] (○).

et al.[44], Devi et al.[26] and from this study results from analysis assuming speed dependence while other not, except for the data from Bordet et al.[42], where the data were analyzed differently depending on the conditions of the experiment. The theoretical values are calculated according to the semiempirical model proposed by Hartmann for the CO_2 line shift[90]. This model, adapted for the CO molecule, takes the following form:

$$\Delta_0\left[\left(\mathrm{v}+\Delta\mathrm{v},J'\right)\leftarrow\left(\mathrm{v},J''\right)\right]= \left(J''-J'\right)\Delta_0^R\left(|m|\right)+a\Delta\mathrm{v}\,\Delta_0^V\left(|m|\right) \quad (4)$$

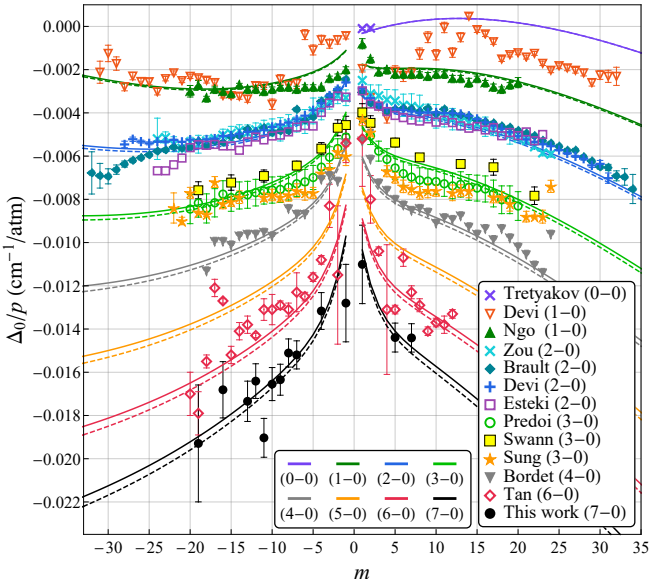

FIG. 9. The experimental and theoretical self-induced pressure shifting coefficients Δ_0/p versus line index m. The values from this work for $(7-0)$ band from the qSDVP LLA analysis (●) are compared to the values for $(0-0)$ band by Tretyakov et al.[44] (×); $(1-0)$ band by Devi et al.[26] (▽) and Ngo et al.[36] (▲); $(2-0)$ band by Zou and Varanasi[29] (×), Devi et al.[34] (+) and Esteki et al.[39] (□), $(3-0)$ band by Predoi-Cross et al.[32] (○), Swann and Gilbert[30] (▣) and Sung and Varanasi[31] (★); $(4-0)$ band by Bordet et al.[42] (▼); $(6-0)$ band by Tan et al.[38] (◇). Solid lines show Δ_0/p values calculated from Eq. (4) and corresponding to the qSDVP while dashed ones correspond to the VP. Details in Section IV B.

where J' is the rotational quantum number of the upper state. Functions $\Delta_0^R\left(|m|\right)$ and $\Delta_0^V\left(|m|\right)$ represent two contributions to the line shift. The first one is purely rotational. The second one is scaled by a factor depending on the vibrational mode, which for a diatomic molecule is simply proportional to $\Delta\mathrm{v}$. They may be modeled by five-parameter functions:

$$\begin{aligned}\Delta_0^R\left(|m|\right)&=\alpha_1^R+\alpha_2^R e^{-|m|\beta_1^R}+\alpha_3^R e^{-|m|\beta_2^R},\\ \Delta_0^V\left(|m|\right)&=\alpha_1^V+\alpha_2^V e^{-|m|\beta_1^V}+\alpha_3^V e^{-|m|\beta_2^V}.\end{aligned} \quad (5)$$

Values of parameters $\alpha_i^{V,R}$ and $\beta_i^{V,R}$ are given in Table IV. These parameters were determined by Hashemi et al.[87] based on experimental data for $(1-0)$[29,36], $(2-0)$[29,91], and $(3-0)$[32] bands and have the same values for the line shifting determined with the VP and speed-dependent profiles. Only the a coefficient in Eq. (4) was determined separately for the case of VP and speed-dependent profiles. For the VP, $a = 0.54$ was determined using $(2-0)$ data[29], and for speed-dependent profiles $a = 0.5$ was retrieved from the fit to the data of the same band measured by Devi et al.[34]. However, the latter value does not reproduce pressure shifting values given in the supplementary material of Ref.[87] and in the HITRAN2020 database[86]. The value of a fitted to the SDV pressure shifting values in HITRAN2020 is $a = 0.529471(23)$. This value agrees with

TABLE IV. Parameters from Ref.[87] used in functions $\Delta_0^R(|m|)$ and $\Delta_0^V(|m|)$ given by Eq. (5).

$\Delta_0^R(\lvert m\rvert)$	$\Delta_0^V(\lvert m\rvert)$
$\alpha_1^R = 2.413\times10^{-2}$	$\alpha_1^V = -2.476\times10^{-2}$
$\alpha_2^R = -8.608\times10^{-2}$	$\alpha_2^V = 1.520\times10^{-3}$
$\alpha_3^R = 6.240\times10^{-2}$	$\alpha_3^V = 2.125\times10^{-2}$
$\beta_1^R = 1.507\times10^{-2}$	$\beta_1^V = 5.363\times10^{-1}$
$\beta_2^R = 2.301\times10^{-2}$	$\beta_2^V = 3.993\times10^{-3}$

the one determined on the basis of our $(7-0)$ measurements: $a = 0.530(8)$.

The results of measurements of $(3-0)$ band by Picque et al.[92] are not shown in the Fig. 9 as they are in agreement within the margins of uncertainty with more recent results of Swann and Gilbert[30] (□). The data for $(4-0)$ band (▼) is acquired in private communication with authors of Bordet et al.[42] and does not have estimation of uncertainty. Uncertainty bars for the data by Tretyakov et al.[44] (×) and from this study (●) show total standard uncertainty (1σ) and one standard statistical uncertainty for the other data. Retrieved in this study Δ_0/p values agree with calculated values for most of the lines within the experimental uncertainty, reflecting the expected shape of its m-dependence, and show good scaling with the vibrational quantum number of the upper level.

V. CONCLUSIONS

We present the first experimental line shape study of $(7-0)$ band of carbon monoxide, located near the 690 nm wavelength range. For 9 transitions the line positions are determined with an accuracy of $3\cdot10^{-4}$ cm^{-1}. Self-pressure broadening and shifting coefficients are determined with a relative uncertainty of about 5%. Collisional narrowing of the spectral line is observed for the first time for such weak transitions and analyzed in terms of speed-dependent effects. Comparison of collisional broadening and shifting coefficients with values extrapolated from prior measurements of lower overtone bands demonstrates good agreement. However, for the $(7-0)$ band we note slightly higher pressure broadening than for the lower overtone bands if SDV profile is used. We verified experimentally a strong dependence of the pressure shifting on the vibrational quantum number. The Hartmann model[90], describing this dependence, was confirmed up to the sixth overtone, which is highly sensitive to the model parameter.

ACKNOWLEDGMENTS

The research was supported by the National Science Centre, Poland project no. 2018/30/E/ST2/00864, 2018/29/B/ST2/02974. S.W. was supported by the National Science Centre, Poland project No. 2021/42/E/ST2/00152. D.L. was supported by the National Science Centre, Poland project No. 2020/39/B/ST2/00719. The research was part of the program of the National Laboratory FAMO in Toruń, Poland. The authors thank Dr. Alain Campargue for providing data on CO $(4-0)$ band pressure shifting coefficients.

AUTHOR DECLARATIONS

Conflict of interest

The authors have no conflicts to disclose.

Author contributions

Aleksandr A. Balashov: Data curation (equal); Formal analysis (lead); Investigation (equal); Software; Visualization; Writing - original draft. Szymon Wójtewicz: Funding acquisition (equal); Investigation (equal); Validation (equal); Writing - review & editing (equal). Jolanta Domysławska: Formal analysis (supporting); Funding acquisition (equal); Investigation (equal); Validation (equal); Writing - review & editing (equal). Roman Ciuryło: Methodology (equal); Validation (equal); Writing - review & editing (equal). Daniel Lisak: Conceptualization (equal); Funding acquisition (equal); Methodology (equal); Supervision (equal); Validation (equal); Writing - review & editing (equal). Katarzyna Bielska: Conceptualization (equal); Data curation (equal); Funding acquisition (equal); Investigation (equal); Supervision (equal); Writing - review & editing (equal).

DATA AVAILABILITY

The data that support the findings of this study are available from the corresponding author upon reasonable request.

[1] T. M. Dame, D. Hartmann, and P. Thaddeus, "The Milky Way in molecular clouds: a new complete CO survey," Astrophys. J. **547**, 792–813 (2001).
[2] R. Visser, E. F. Dishoeck, and J. H. Black, "The photodissociation and chemistry of CO isotopologues: applications to interstellar clouds and circumstellar disks*," Astron. Astrophys. **503**, 323–343 (2009).
[3] P. Connes, J. Connes, L. D. Kaplan, and W. S. Benedict, "Carbon monoxide in Venus atmosphere," Astrophys. J. **152**, 731–743 (1968).
[4] E. Marcq, F. P. Mills, C. D. Parkinson, and A. C. Vandaele, "Composition and Chemistry of the Neutral Atmosphere of Venus," Space Sci. Rev. **214**, 10 (2018).
[5] T. Owen, K. Biemann, D. R. Rushneck, J. E. Biller, D. W. Howarth, and A. L. Lafleur, "The composition of the atmosphere at the surface of Mars," J. Geophys. Res. **82**, 4635–4639 (1977).
[6] K. S. Olsen, F. Lefevre, F. Montmessin, A. A. Fedorova, A. Trokhimovskiy, L. Baggio, O. Korablev, J. Alday, C. F. Wilson, F. Forget, D. A. Belyaev, A. Patrakeev, A. V. Grigoriev, and A. Shakun, "The vertical structure of CO in the Martian atmosphere from the ExoMars Trace Gas Orbiter," Nat. Geosci. **14**, 67–71 (2021).
[7] M. R. Swain, P. Deroo, C. A. Griffith, G. Tinetti, A. Thatte, G. Vasisht, P. Chen, J. Bouwman, I. J. Crossfield, D. Angerhausen, C. Afonso, and T. Henning, "A ground-based near-infrared emission spectrum of the exoplanet HD 189733b," Nature **463**, 637–639 (2010).
[8] D. Grant, J. D. Lothringer, H. R. Wakeford, M. K. Alam, L. Alderson, J. L. Bean, B. Benneke, J.-M. Desert, T. Daylan, L. Flagg, R. Hu, J. Inglis, J. Kirk, L. Kreidberg, M. Lopez-Morales, L. Mancini, T. Mikal-Evans,

K. Molaverdikhani, E. Palle, B. Rackham, V, S. Redfield, K. B. Stevenson, J. A. Valenti, N. L. Wallack, K. Aggarwal, E.-M. Ahrer, I. J. M. Crossfield, N. Crouzet, N. Iro, N. K. Nikolov, P. Wheatley, and J. T. E. Communit, "Detection of Carbon Monoxide's 4.6 Micron Fundamental Band Structure in WASP-39b's Atmosphere with JWST NIRSpec G395H," Astrophys. J. Lett. **949**, L15 (2023).

[9] C. Wang and P. Sahay, "Breath analysis using laser spectroscopic techniques: breath biomarkers, spectral fingerprints, and detection limits," Sensors **9**, 8230–8262 (2009).

[10] P. J. Crutzen, L. E. Heidt, J. P. Krasnec, W. H. Pollock, and W. Seiler, "Biomass burning as a source of atmospheric gases CO, H_2, N_2O, NO, CH_3Cl and COS," Nature **282**, 253–256 (1979).

[11] L. Böhler, G. Görtler, J. Krail, and M. Kozek, "Carbon monoxide emission models for small-scale biomass combustion of wooden pellets," Appl. Energy **254**, 113668 (2019).

[12] V. S. Rakitin, N. F. Elansky, A. I. Skorokhod, A. V. Dzhola, A. V. Rakitina, A. V. Shilkin, N. S. Kirillova, and A. V. Kazakov, "Long-Term Tendencies of Carbon Monoxide in the Atmosphere of the Moscow Megapolis," Izv. Atmos. Oceanic Phys. **57**, 116–125 (2021).

[13] C. G. MacDonald, J.-P. Mastrogiacomo, J. L. Laughner, J. K. Hedelius, R. Nassar, and D. Wunch, "Estimating enhancement ratios of nitrogen dioxide, carbon monoxide and carbon dioxide using satellite observations," Atmos. Chem. Phys. **23**, 3493–3516 (2023).

[14] J. R. Rozante, V. Rozante, D. Souza Alvim, A. Ocimar Manzi, J. Barboza Chiquetto, M. T. Siqueira D'Amelio, and D. S. Moreira, "Variations of carbon monoxide concentrations in the megacity of São Paulo from 2000 to 2015 in different time scales," Atmosphere **8**, 81 (2017).

[15] D. Bruhn, K. R. Albert, T. N. Mikkelsen, and P. Ambus, "UV-induced carbon monoxide emission from living vegetation," Biogeosciences **10**, 7877–7882 (2013).

[16] L. Conte, S. Szopa, R. Séférian, and L. Bopp, "The oceanic cycle of carbon monoxide and its emissions to the atmosphere," Biogeosciences **16**, 881–902 (2019).

[17] S. Hameed, R. D. Cess, and J. S. Hogan, "Response of the global climate to changes in atmospheric chemical composition due to fossil fuel burning," J. Geophys. Res. Oceans **85**, 7537–7545 (1980).

[18] D. Johnson and G. Marston, "The gas-phase ozonolysis of unsaturated volatile organic compounds in the troposphere," Chem. Soc. Rev. **37**, 699–716 (2008).

[19] J. R. Drummond, J. Zou, F. Nichitiu, J. Kar, R. Deschambaut, and J. Hackett, "A review of 9-year performance and operation of the MOPITT instrument," Advan. Sp. Res. **45**, 760–774 (2010).

[20] P. F. Bernath, "The atmospheric chemistry experiment (ACE)," J. Quant. Spectrosc. Radiat. Transf. **186**, 3–16 (2017).

[21] J. Veefkind, I. Aben, K. McMullan, H. Förster, J. de Vries, G. Otter, J. Claas, H. J. Eskes, J. F. de Haan, Q. Kleipool, M. van Weele, O. Hasekamp, R. Hoogeveen, J. Landgraf, R. Snel, P. Tol, P. Ingmann, R. Voors, B. Kruizinga, R. Vink, H. Visser, and P. F. Levelt, "TROPOMI on the ESA Sentinel-5 precursor: a GMES mission for global observations of the atmospheric composition for climate, air quality and ozone layer applications," Rem. Sens. Environ. **120**, 70–83 (2012).

[22] M. D. Mazière, A. M. Thompson, M. J. Kurylo, J. D. Wild, G. Bernhard, T. Blumenstock, G. O. Braathen, J. W. Hannigan, J.-C. Lambert, T. Leblanc, T. J. McGee, G. Nedoluha, I. Petropavlovskikh, G. Seckmeyer, P. C. Simon, W. Steinbrecht, and S. E. Strahan, "The Network for the Detection of Atmospheric Composition Change (NDACC): history, status and perspectives," Atmos. Chem. Phys. **18**, 4935–4964 (2018).

[23] D. Wunch, G. C. Toon, J. F. Blavier, R. A. Washenfelder, J. Notholt, B. J. Connor, D. W. Griffith, V. Sherlock, and P. O. Wennberg, "The Total Carbon Column Observing Network," Philos. Trans., Math. Phys. Eng. Sci. **369**, 2087–2112 (2011).

[24] M. Frey, M. K. Sha, F. Hase, M. Kiel, T. Blumenstock, R. Harig, G. Surawicz, N. M. Deutscher, K. Shiomi, J. E. Franklin, H. Bösch, J. Chen, M. Grutter, H. Ohyama, Y. Sun, A. Butz, G. M. Tsidu, D. Ene, D. Wunch, Z. Cao, O. Garcia, M. Ramonet, F. Vogel, and J. Orphal, "Building the COllaborative Carbon Column Observing Network (COCCON): long-term stability and ensemble performance of the EM27/SUN Fourier transform spectrometer," Atmos. Meas. Tech. **12**, 1513–1530 (2019).

[25] G. Herzberg and K. N. Rao, "Rotation-Vibration Spectra of Diatomic and Simple Polyatomic Molecules with Long Absorbing Paths. II. The Spectrum of Carbon Monoxide below 1.2μ," J. Chem. Phys. **17**, 1099–1102 (1949).

[26] V. M. Devi, D. C. Benner, M. A. H. Smith, and C. P. Risland, "Self-broadening and self-shift coefficients in the fundamental band of $^{12}C^{16}O$," J. Quant. Spectrosc. Radiat. Transf. **60**, 815–824 (1998).

[27] J. Henningsen, H. Simonsen, T. Møgelberg, and E. Trudsø, "The $0 \rightarrow 3$ Overtone Band of CO: Precise Linestrengths and Broadening Parameters," J. Mol. Spectrosc. **193**, 354–362 (1999).

[28] D. Jacquemart, J.-Y. Mandin, V. Dana, N. Picqué, and G. Guelachvili, "A multispectrum fitting procedure to deduce molecular line parameters: Application to the $3-0$ band of $^{12}C^{16}O$," Eur. Phys. J. D **14**, 55–69 (2001).

[29] Q. Zou and P. Varanasi, "New laboratory data on the spectral line parameters in the $1-0$ and $2-0$ bands of $^{12}C^{16}O$ relevant to atmospheric remote sensing," J. Quant. Spectrosc. Radiat. Transf. **75**, 63–92 (2002).

[30] W. C. Swann and S. L. Gilbert, "Pressure-induced shift and broadening of $1560-1630$-nm carbon monoxide wavelength-calibration lines," J. Opt. Soc. Am. B **19**, 2461–2467 (2002).

[31] K. Sung and P. Varanasi, "Intensities, collision-broadened half-widths, and collision-induced line shifts in the second overtone band of $^{12}C^{16}O$," J. Quant. Spectrosc. Radiat. Transf. **83**, 445–458 (2004).

[32] A. Predoi-Cross, C. Hnatovsky, K. Strong, J. R. Drummond, and D. C. Benner, "Temperature dependence of self- and N_2-broadening and pressure-induced shifts in the $3\leftarrow0$ band of CO," J. Mol. Struct. **695-696**, 269–286 (2004), Winnewisser Special Issue.

[33] G. S. Engel, W. S. Drisdell, F. N. Keutsch, E. J. Moyer, and J. G. Anderson, "Ultra-sensitive near-infrared integrated cavity output spectroscopy technique for detection of CO at 1.57 μm: new sensitivity limits for absorption measurements in passive optical cavities," Appl. Opt. **45**, 9221–9229 (2006).

[34] V. M. Devi, D. C. Benner, M. A. H. Smith, A. W. Mantz, K. Sung, L. R. Brown, and A. Predoi-Cross, "Spectral line parameters including temperature dependences of self- and air-broadening in the $2\leftarrow0$ band of CO at 2.3μm," J. Quant. Spectrosc. Radiat. Transf. **113**, 1013–1033 (2012), three Leaders in Spectroscopy.

[35] S. Wójtewicz, K. Stec, P. Masłowski, A. Cygan, D. Lisak, R. S. Trawiński, and R. Ciuryło, "Low pressure line-shape study of self-broadened CO transitions in the $(3\leftarrow0)$ band," J. Quant. Spectrosc. Radiat. Transf. **130**, 191–200 (2013), HITRAN2012 special issue.

[36] N. H. Ngo, X. Landsheere, E. Pangui, S. B. Morales, H. Tran, and J.-M. Hartmann, "Self-broadening and -shifting of very intense lines of the $1\leftarrow0$ band of $^{12}C^{16}O$," J. Quant. Spectrosc. Radiat. Transf. **149**, 285–290 (2014).

[37] A. Campargue, E. V. Karlovets, and S. Kassi, "The $4-0$ band of carbon monoxide by high sensitivity Cavity Ring Down spectroscopy near 8200 cm^{-1}," J. Quant. Spectrosc. Radiat. Transf. **154**, 113–119 (2015).

[38] Y. Tan, J. Wang, X.-Q. Zhao, A.-W. Liu, and S.-M. Hu, "Cavity ring-down spectroscopy of the fifth overtone of CO," J. Quant. Spectrosc. Radiat. Transf. **187**, 274–279 (2017).

[39] K. Esteki, A. Predoi-Cross, C. Povey, S. Ivanov, A. Ghoufi, F. Thibault, and M. A. H. Smith, "Room temperature self- and H_2-broadened line parameters of carbon monoxide in the first overtone band: Theoretical and revised experimental results," J. Quant. Spectrosc. Radiat. Transf. **203**, 309–324 (2017).

[40] Yu. G. Borkov, A. M. Solodov, T. M. Petrova, A. A. Solodov, E. V. Karlovets, and V. I. Perevalov, "Fourier transforms CO spectra near 1.19 μm," J. Quant. Spectrosc. Radiat. Transf. **242**, 106790 (2020).

[41] Yu. G. Borkov, A. M. Solodov, A. A. Solodov, T. M. Petrova, E. V. Karlovets, and V. I. Perevalov, "Fourier transform CO spectra near 1.6 μm," J. Quant. Spectrosc. Radiat. Transf. **253**, 107064 (2020).

[42] B. Bordet, S. Kassi, and A. Campargue, "Line parameters of the $4-0$ band of carbon monoxide by high sensitivity cavity ring down spectroscopy near 1.2 μm," J. Quant. Spectrosc. Radiat. Transf. **260**, 107453 (2021).

[43] K. Bielska, A. A. Kyuberis, Z. D. Reed, G. Li, A. Cygan, R. Ciuryło, E. M. Adkins, L. Lodi, N. F. Zobov, V. Ebert, D. Lisak, J. T. Hodges, J. Tennyson, and O. L. Polyansky, "Subpromille Measurements and Calculations of CO $(3-0)$ Overtone Line Intensities," Phys. Rev. Lett. **129**, 043002 (2022).

[44] M. Yu. Tretyakov, E. A. Serov, D. S. Makarov, I. N. Vilkov, G. Y. Golubiatnikov, T. A. Galanina, M. A. Koshelev, A. A. Balashov, A. A. Simonova, and F. Thibault, "Pure rotational R(0) and R(1) lines of CO in Ar baths: experimental broadening, shifting and mixing parameters in a wide pressure range *versus ab initio* calculations," Phys. Chem. Chem. Phys. **25**, 1310–1330 (2023).

[45] J. A. Coxon and P. G. Hajigeorgio, "Direct potential fit analysis of the $X^1\Sigma^+$ ground state of CO," J. Chem. Phys. **121**, 2992–3008 (2004).

[46] T. I. Velichko, S. N. Mikhailenko, and S. A. Tashkun, "Global multi-isotopologue fit of measured rotation and vibration-rotation line positions of CO in $X^1\Sigma^+$ state and new set of mass-independent Dunham coefficients," J. Quant. Spectrosc. Radiat. Transf. **113**, 1643–1655 (2012).

[47] G. Li, I. E. Gordon, L. S. Rothman, Y. Tan, S.-M. Hu, S. Kassi, A. Campargue, and E. S. Medvedev, "Rovibrational line lists for nine isotopologues of the CO molecule in the $X^1\Sigma^+$ ground electronic state," Astrophys. J. Suppl. Ser. **216**, 15 (2015).

[48] V. V. Meshkov, A. Y. Ermilov, A. V. Stolyarov, E. S. Medvedev, V. G. Ushakov, and I. E. Gordon, "Semi-empirical dipole moment of carbon monoxide and line lists for all its isotopologues revisited," J. Quant. Spectrosc. Radiat. Transf. **280**, 108090 (2022).

[49] A. A. Balashov, K. Bielska, G. Li, A. A. Kyuberis, S. Wójtewicz, J. Domysławska, R. Ciuryło, N. F. Zobov, D. Lisak, J. Tennyson, and O. L. Polyansky, "Measurement and calculation of CO (7-0) overtone line intensities," J. Chem. Phys. **158**, 234306 (2023).

[50] T. Zelevinsky, S. Kotochigova, and J. Ye, "Precision test of mass-ratio variations with lattice-confined ultracold molecules," Phys. Rev. Lett. **100**, 043201 (2008).

[51] D. N. B. Hall, "Detection of the ^{13}C, ^{17}O, and ^{18}O isotope bands of CO in the infrared solar spectrum," Astrophys. J. **182**, 977–982 (1973).

[52] N. M. Förster Schreiber, "Moderate-Resolution Near-Infrared Spectroscopy of Cool Stars: A New K-Band Library," Astron. J. **120**, 2089 (2000).

[53] M. G. Berthoud, L. D. Keller, T. L. Herter, M. J. Richter, and D. G. Whelan, "Near-IR CO Overtone Emission in 51 Ophiuchi," Astrophys. J. **660**, 461–468 (2007).

[54] F. Martins, M. Pomarès, L. Deharveng, A. Zavagno, and J. C. Bouret, "Near-IR integral field spectroscopy of ionizing stars and young stellar objects on the borders of H II regions," Astron. Astrophys. **510**, A32 (2010).

[55] GRAVITY Collaboration, A. Caratti o Garatti, R. Fedriani, R. Garcia Lopez, M. Koutoulaki, K. Perraut, H. Linz, W. Brandner, P. Garcia, L. Klarmann, T. Henning, L. Labadie, J. Sanchez-Bermudez, B. Lazareff, E. F. van Dishoeck, P. Caselli, P. T. de Zeeuw, A. Bik, M. Benisty, C. Dougados, T. P. Ray, A. Amorim, J.-P. Berger, Y. Clénet, V. Coudé du Foresto, G. Duvert, A. Eckart, F. Eisenhauer, F. Gao, E. Gendron, R. Genzel, S. Gillessen, P. Gordo, L. Jocou, M. Horrobin, P. Kervella, S. Lacour, J.-B. Le Bouquin, P. Léna, R. Grellmann, T. Ott, T. Paumard, G. Perrin, G. Rousset, S. Scheithauer, J. Shangguan, J. Stadler, O. Straub, C. Straubmeier, E. Sturm, W. F. Thi, F. H. Vincent, and F. Widmann, "The GRAVITY young stellar object survey - II. First spatially resolved observations of the CO bandhead emission in a high-mass YSO," Astron. Astrophys. **635**, L12 (2020).

[56] Á. Kóspál, P. Ábrahám, M. Goto, Zs. Regály, C. P. Dullemond, Th. Henning, A. Juhász, A. Sicilia-Aguilar, and M. van den Ancker, "Near-infrared spectroscopy of EX Lupi in outburst," Astrophys. J. **736**, 72 (2011).

[57] A. W. Mantz and J.-P. Maillard, "Emission spectra with a high resolution Fourier transform spectrometer: CO spectra and their astrophysical importance," J. Mol. Spectrosc. **53**, 466–478 (1974).

[58] E. S. Medvedev and V. G. Ushakov, "Effect of the analytical form of the dipole-moment function on the rotational intensity distributions in the high-overtone vibrational bands of carbon monoxide," J. Quant. Spectrosc. Radiat. Transf. **272**, 107803 (2021).

[59] K. Bielska, J. Domysławska, S. Wójtewicz, A. Balashov, M. Słowiński, M. Piwiński, A. Cygan, R. Ciuryło, and D. Lisak, "Simultaneous observation of speed dependence and Dicke narrowing for self-perturbed P-branch lines of O_2 B band," J. Quant. Spectrosc. Radiat. Transf. **276**, 107927 (2021).

[60] R. W. P. Drever, J. L. Hall, F. V. Kowalski, J. Hough, G. M. Ford, A. J. Munley, and H. Ward, "Laser phase and frequency stabilization using an optical resonator," Appl. Phys. B **31**, 97–105 (1983).

[61] M. Zhu and J. L. Hall, "Stabilization of optical phase/frequency of a laser system: application to a commercial dye laser with an external stabilizer," J. Opt. Soc. Am. B **10**, 802–816 (1993).

[62] J. T. Hodges, H. P. Layer, W. W. Miller, and G. E. Scace, "Frequency-stabilized single-mode cavity ring-down apparatus for high-resolution absorption spectroscopy," Rev. Sci. Instrum. **75**, 849–863 (2004).

[63] P. Morzyński, M. Bober, D. Bartoszek-Bober, J. Nawrocki, P. Krehlik, Ł. Śliwczyński, M. Lipiński, P. Masłowski, A. Cygan, P. Dunst, M. Garus, D. Lisak, J. Zachorowski, W. Gawlik, C. Radzewicz, R. Ciuryło, and M. Zawada, "Absolute measurement of the $^1S_0 - ^3P_0$ clock transition in neutral ^{88}Sr over the 330 km-long stabilized fibre optic link," Sci. Rep. **5**, 17495 (2015).

[64] P. Krehlik, Ł. Śliwczyński, Ł. Buczek, J. Kołodziej, and M. Lipiński, "Ultrastable long-distance fibre-optic time transfer: active compensation over a wide range of delays," Metrologia **52**, 82–88 (2015).

[65] A. Cygan, S. Wójtewicz, G. Kowzan, M. Zaborowski, P. Wcisło, J. Nawrocki, P. Krehlik, Ł. Śliwczyński, M. Lipiński, P. Masłowski, R. Ciuryło, and D. Lisak, "Absolute molecular transition frequencies measured by three cavity-enhanced spectroscopy techniques," J. Chem. Phys. **144**, 214202 (2016).

[66] Z. Jiang, A. Czubla, J. Nawrocki, W. Lewandowski, and E. F. Arias, "Comparing a GPS time link calibration with an optical fibre self-calibration with 200 ps accuracy," Metrologia **52**, 384 (2015).

[67] P. R. Berman, "Speed-dependent collisional width and shift parameters in spectral profiles," J. Quant. Spectrosc. Radiat. Transf. **12**, 1331–1342 (1972).

[68] F. Rohart, H. Mäder, and H. Nicolaisen, "Speed dependence of rotational relaxation induced by foreign gas collisions: Studies on CH_3F by millimeter wave coherent transients," J. Chem. Phys. **101**, 6475–6486 (1994).

[69] B. Lance, G. Blanquet, J. Walrand, and J.-P. Bouanich, "On the Speed-Dependent Hard Collision Lineshape Models: Application to C_2H_2Perturbed by Xe," J. Mol. Spectrosc. **185**, 262–271 (1997).

[70] A. S. Pine, "Asymmetries and correlations in speed-dependent Dicke-narrowed line shapes of argon-broadened HF," J. Quant. Spectrosc. Radiat. Transf. **62**, 397–423 (1999).

[71] N. Ngo, D. Lisak, H. Tran, and J.-M. Hartmann, "An isolated line-shape model to go beyond the Voigt profile in spectroscopic databases and radiative transfer codes," J. Quant. Spectrosc. Radiat. Transf. **129**, 89–100 (2013).

[72] J. Tennyson, P. F. Bernath, A. Campargue, A. G. Császár, L. Daumont, R. R. Gamache, J. T. Hodges, D. Lisak, O. V. Naumenko, L. S. Rothman, H. Tran, N. F. Zobov, J. Buldyreva, C. D. Boone, M. D. De Vizia, L. Gianfrani, J.-M. Hartmann, R. McPheat, D. Weidmann, J. Murray, N. H. Ngo, and O. L. Polyansky, "Recommended isolated-line profile for representing high-resolution spectroscopic transitions (IUPAC technical report)," Pure Appl. Chem. **86**, 1931–1943 (2014).

[73] P. Wcisło, I. E. Gordon, H. Tran, Y. Tan, S.-M. Hu, A. Campargue, S. Kassi, D. Romanini, C. Hill, R. V. Kochanov, and L. S. Rothman, "The implementation of non-Voigt line profiles in the HITRAN database: H_2 case study," J. Quant. Spectrosc. Radiat. Transf. **177**, 75–91 (2016).

[74] D. C. Benner, C. P. Rinsland, V. M. Devi, M. A. H. Smith, and D. Atkins, "A multispectrum nonlinear least squares fitting technique," J. Quant. Spectrosc. Radiat. Transf. **53**, 705–721 (1995).

[75] A. S. Pine and R. Ciuryło, "Multispectrum Fits of Ar-Broadened HF with a Generalized Asymmetric Lineshape: Effects of Correlation, Hardness, Speed Dependence, and Collision Duration," J. Mol. Spectrosc. **208**, 180–187 (2001).

[76] D. Lisak, J. T. Hodges, and R. Ciuryło, "Comparison of semiclassical line-shape models to rovibrational H_2O spectra measured by frequency-stabilized cavity ring-down spectroscopy," Phys. Rev. A **73**, 012507 (2006).

[77] M. Nelkin and A. Ghatak, "Simple Binary Collision Model for Van Hove's $G_s(r,t)$," Phys. Rev. **135**, A4–A9 (1964).

[78] D. Priem, J.-M. Colmont, F. Rohart, G. Wlodarczak, and R. R. Gamache, "Relaxation and Lineshape of the 500.4-GHz Line of Ozone Perturbed by N_2 and O_2," J. Mol. Spectrosc. **204**, 204–215 (2000).

[79] S. Wójtewicz, A. Cygan, P. Masłowski, J. Domysławska, D. Lisak, R. S. Trawiński, and R. Ciuryło, "Spectral line shapes of self-broadened P-

branch transitions of oxygen *B* band," J. Quant. Spectrosc. Radiat. Transf. **144**, 36–48 (2014).

[80] A. Cygan, D. Lisak, S. Wójtewicz, J. Domysławska, J. T. Hodges, R. S. Trawiński, and R. Ciuryło, "High-signal-to-noise-ratio laser technique for accurate measurements of spectral line parameters," Phys. Rev. A **85**, 022508 (2012).

[81] T. Q. Bui, D. A. Long, A. Cygan, V. T. Sironneau, D. W. Hogan, P. M. Rupasinghe, R. Ciuryło, D. Lisak, and M. Okumura, "Observations of Dicke narrowing and speed dependence in air-broadened CO_2 lineshapes near 2.06 μm," J. Chem. Phys. **141**, 174301 (2014).

[82] J. Courtois and J. T. Hodges, "Coupled-cavity ring-down spectroscopy technique," Opt. Lett. **37**, 3354–3356 (2012).

[83] R. W. Fox and L. Hollberg, "Role of spurious reflections in ring-down spectroscopy," Opt. Lett. **27**, 1833–1835 (2002).

[84] S. Bell, "Measurement good practice guide no. 11," (National Physical Laboratory, Teddington, Middlesex, United Kingdom, TW11 0LW, 2001) Chap. 7.1.2, p. 13, issue 2 ed.

[85] P. Rosenkranz, "Shape of the 5 mm oxygen band in the atmosphere," IEEE Trans. Antennas Propag. **23**, 498–506 (1975).

[86] I. E. Gordon, L. S. Rothman, R. J. Hargreaves, R. Hashemi, E. V. Karlovets, F. M. Skinner, E. K. Conway, C. Hill, R. V. Kochanov, Y. Tan, P. Wcisło, A. A. Finenko, K. Nelson, P. F. Bernath, M. Birk, V. Boudon, A. Campargue, K. V. Chance, A. Coustenis, B. J. Drouin, J.-M. Flaud, R. R. Gamache, J. T. Hodges, D. Jacquemart, E. J. Mlawer, A. V. Nikitin, V. I. Perevalov, M. Rotger, J. Tennyson, G. C. Toon, H. Tran, V. G. Tyuterev, E. M. Adkins, A. Baker, A. Barbe, E. Canè, A. G. Császár, A. Dudaryonok, O. Egorov, A. J. Fleisher, H. Fleurbaey, A. Foltynowicz, T. Furtenbacher, J. J. Harrison, J. Hartmann, V. Horneman, X. Huang, T. Karman, J. Karns, S. Kassi, I. Kleiner, V. Kofman, F. Kwabia–Tchana, N. N. Lavrentieva, T. J. Lee, D. A. Long, A. A. Lukashevskaya, O. M. Lyulin, V. Yu. Makhnev, W. Matt, S. T. Massie, M. Melosso, S. N. Mikhailenko, D. Mondelain, H. S. P. Müller, O. V. Naumenko, A. Perrin, O. L. Polyansky, E. Raddaoui, P. L. Raston, Z. D. Reed, M. Rey, C. Richard, R. Tóbiás, I. Sadiek, D. W. Schwenke, E. Starikova, K. Sung, F. Tamassia, S. A. Tashkun, J. Vander Auwera, I. A. Vasilenko, A. A. Vigasin, G. L. Villanueva, B. Vispoel, G. Wagner, A. Yachmenev, and S. N. Yurchenko, "The HITRAN2020 molecular spectroscopic database," J. Quant. Spectrosc. Radiat. Transf. **277**, 107949 (2022).

[87] R. Hashemi, I. E. Gordon, E. M. Adkins, J. T. Hodges, D. A. Long, M. Birk, J. Loos, C. D. Boone, A. J. Fleisher, A. Predoi-Cross, and L. S. Rothman, "Improvement of the spectroscopic parameters of the air- and self-broadened NO and CO lines for the HITRAN2020 database applications," J. Quant. Spectrosc. Radiat. Transf. **271**, 107735 (2021).

[88] E. S. Medvedev and V. G. Ushakov, "Irregular semi-empirical dipole-moment function for carbon monoxide and line lists for all its isotopologues verified for extremely high overtone transitions," J. Quant. Spectrosc. Radiat. Transf. **288**, 108–255 (2022).

[89] A. Predoi-Cross, J. P. Bouanich, D. C. Benner, A. D. May, and J. R. Drummond, "Broadening, shifting, and line asymmetries in the 2←0 band of CO and $CO-N_2$: Experimental results and theoretical calculations," J. Chem. Phys. **113**, 158–168 (2000).

[90] J.-M. Hartmann, "A simple empirical model for the collisional spectral shift of air-broadened CO_2 lines," J. Quant. Spectrosc. Radiat. Transf. **110**, 2019–2026 (2009).

[91] V. M. Devi, A. Predoi-Cross, D. C. Benner, M. Smith, C. Rinsland, and A. Mantz, "Self- and H_2-broadened width and shift coefficients in the 2←0 band of $^{12}C^{16}O$: revisited," J. Mol. Spectrosc. **228**, 580–592 (2004).

[92] N. Picqué, G. Guelachvili, V. Dana, and J. Y. Mandin, "Absolute line intensities, vibrational transition moment, and self-broadening coefficients for the 3−0 band of $^{12}C^{16}O$," J. Mol. Spectrosc. **517**, 427–434 (2000).